Supporting Information

Hu et al. 10.1073/pnas.1305766110

SI Text

Model and Simulations

Simulation Method. We have performed dissipative particle dynamics (DPD) simulations (1–3). DPD is a coarse-grained molecular dynamics technique that explicitly includes water (3). The DPD particles, or "beads," represent either a number of identical molecules or several molecular groups, rather than single atoms. The internal degrees of freedom of these molecules or molecular groups are reflected by dissipative forces and random forces, and the chemical nature of the molecules and molecular groups—for example, their hydrophobicity and hydrophilicity—is taken into account by conservative forces. Because all forces conserve momentum, DPD reproduces the correct hydrodynamics (3).

The DPD force that a bead j exerts on a bead i is the sum of three pairwise-additive forces: (*i*) the conservative force $\mathbf{F}_{ij}^{C}$, which results from bonded and nonbonded interactions of the beads; (*ii*) the dissipative or viscous friction force $\mathbf{F}_{ij}^{D}$; and (*iii*) the random force $\mathbf{F}_{ij}^{R}$. The dissipative force $\mathbf{F}_{ij}^{D}$ is related to the relative velocity $\mathbf{v}_{ij} = \mathbf{v}_i - \mathbf{v}_j$ of the beads via

$$\mathbf{F}_{ij}^{D} = \begin{cases} -\gamma_{ij}(1 - r_{ij}/r_0)^2 (\hat{\mathbf{r}}_{ij} \cdot \mathbf{v}_{ij})\hat{\mathbf{r}}_{ij}, & r_{ij} < r_0 \\ 0, & r_{ij} \geq r_0 \end{cases} \quad \textbf{[S1]}$$

with a friction coefficient $\gamma_{ij} = \gamma_{ji}$ that depends on the bead type. Here, $r_{ij} = |\mathbf{r}_i - \mathbf{r}_j|$ denotes the distance between the beads, $\hat{\mathbf{r}}_{ij} = (\mathbf{r}_i - \mathbf{r}_j)/r_{ij}$ is the unit vector pointing from bead j to bead i, and r_0 is the diameter of the beads. The random force $\mathbf{F}_{ij}^{R}$ representing thermal noise has the form:

$$\mathbf{F}_{ij}^{R} = \begin{cases} \sqrt{2\gamma_{ij}k_B T}(1 - r_{ij}/r_0)\zeta_{ij}\hat{\mathbf{r}}_{ij}, & r_{ij} < r_0 \\ 0, & r_{ij} \geq r_0 \end{cases} . \quad \textbf{[S2]}$$

Here, k_B is Boltzmann's constant, T is the temperature, and the Gaussian white-noise ζ_{ij} satisfies the stochastic properties $\langle \zeta_{ij}(t) \rangle = 0$ and $\langle \zeta_{ij}(t)\zeta_{i'j'}(t') \rangle = (\delta_{ii'}\delta_{jj'} + \delta_{ij'}\delta_{ji'})\delta(t - t')$ as well as the symmetry property $\zeta_{ij}(t) = \zeta_{ji}(t)$.

Bonded Interactions. Our coarse-grained model includes water, lipid molecules, and receptor and ligand molecules. Water molecules (W) are represented by single beads. A lipid molecule consists of three hydrophilic head beads (H) and two hydrophobic chains (C) with four beads each (4–7) (Fig. 1*A*). Adjacent beads are connected via harmonic potentials

$$V_{\text{bond}}(r) = \frac{1}{2}k_r(r - l_0)^2, \quad \textbf{[S3]}$$

with bond strength $k_r = 128\, k_B T/r_0^2$ and preferred bond length $l_0 = 0.5\, r_0$ (5). Here, r is the distance between the two beads. The two hydrophobic chains of the lipid molecules are stiffened by the bending potential (4)

$$V_{\text{bend}}(\phi) = k_\phi[1 - \cos(\phi - \phi_0)] \quad \textbf{[S4]}$$

that acts between two consecutive bonds along each chain. The bending constant is $k_\phi = 15\, k_B T$, and the bond angle ϕ attains the preferred value $\phi_0 = 0$ for collinear bonds (6, 7).

The anchored receptor and ligand molecules consist of a trans-membrane segment and an interaction segment (Fig. 1*A*). The transmembrane segment is composed of four layers of lipid-chain–like beads (T_C), which are shown in yellow in Fig. 1*A*, in between two layers of lipid-head–like beads (T_H) shown in blue. The interaction segment consists of six layers of a hydrophilic bead type I. Each pair of nearest neighboring beads of a receptor or ligand is connected by a harmonic potential with bond strength $k_r = 128\, k_B T/r_0^2$ and bond length $l_0 = 0.875\, r_0$. This bond length corresponds to the average distance of neighboring water beads in our simulations with bead density $\rho = 3\, r_0^{-3}$. Each pair of next-nearest neighboring beads in two adjacent layers of a receptor or ligand is connected by a harmonic potential with bond strength $k_r = 128\, k_B T/r_0^2$ and bond length $l_0 = \sqrt{2} \times 0.875\, r_0$.

Nonbonded Interactions. In addition to the forces resulting from the bonded interactions specified above, all pairs of DPD beads—except for the interaction beads of a receptor and a ligand—exhibit the soft repulsive forces

$$\mathbf{F}_{ij}^{C} = \begin{cases} a_{ij}(1 - r_{ij}/r_0)\hat{\mathbf{r}}_{ij} & r_{ij} < r_0 \\ 0, & r_{ij} \geq r_0 \end{cases} \quad \textbf{[S5]}$$

with a repulsion strength a_{ij} that depends on the types of the two beads i and j (Table S1). The different repulsion strengths reflect the chemical nature of the beads—that is, their hydrophobicity or hydrophilicity. To avoid a clustering of receptors and ligands, the repulsion strength between the beads of two different receptors or two different ligands adopts the value $a_{ij} = 75\, k_B T/r_0$, which is larger than the repulsion strength $a_{ij} = 25\, k_B T/r_0$ between two beads of the same receptor, same ligand, or a receptor and a ligand. The friction coefficient γ_{ij} of the dissipative forces given by Eq. **S1** between two beads is affected by their repulsion strength as (5):

$$\gamma_{ij} = \begin{cases} 4.5, & a_{ij} < 35 \\ 9.0, & 35 \leq a_{ij} < 75 \\ 20.0, & a_{ij} \geq 75 \end{cases} . \quad \textbf{[S6]}$$

The friction coefficient is given here in units of $\sqrt{m_0 k_B T/r_0^2}$, where m_0 is the bead mass.

The specific binding of a receptor and a ligand molecule is modeled via the binding potential

$$V_{\text{bind}}(r, \theta) = v_{\text{bind}}(r)e^{-k_\theta(\theta - \theta_0)^2}, \quad \textbf{[S7]}$$

which depends both on the distance r between the interaction beads of the receptors and ligands and on the angle θ between the two molecules. The interaction beads are located in the center of the top layer of the receptors' and ligands' interaction regions and are indicated in black in Fig. 1*A*. The angle θ between a receptor and a ligand molecule is defined as the angle between the two bonds that connect the interaction beads of the molecules to the central beads of the adjacent bead layers. The distance-dependent term $v_{\text{bind}}(r)$ of the specific interaction is

$$v_{\text{bind}}(r) = \begin{cases} \frac{1}{2}r_0(a_{\text{II}}(1 - r/r_0)^2 - F_m), & r < r_0 \\ F_m r_0((1 - r/r_0)^2 - \frac{1}{2}), & r_0 \leq r < \frac{3}{2}r_0 \\ -F_m r_0(2 - r/r_0)^2, & \frac{3}{2}r_0 \leq r < 2r_0 \\ 0, & r \geq 2r_0 \end{cases} \quad \textbf{[S8]}$$

with the DPD repulsion strength $a_{II} = 25\, k_B T/r_0$ and the attraction strength $F_m = 16\, k_B T/r_0$ (Fig. S1A). Differentiating $v_{bind}(r)$ with respect to r leads to the radial force component

$$F_{bind}(r) = \begin{cases} a_{II}(1 - r/r_0), & r < r_0 \\ 2F_m(1 - r/r_0), & r_0 \leq r < \frac{3}{2}r_0 \\ 2F_m(r/r_0 - 2), & \frac{3}{2}r_0 \leq r < 2r_0 \\ 0, & r \geq 2r_0 \end{cases}, \qquad \textbf{[S9]}$$

which includes a soft repulsion for $r < r_0$ and an attraction for $r_0 \leq r < 2\, r_0$ (Fig. S1B). The parameter k_θ in the binding potential S7 determines the width of the binding angle distribution and is chosen to be $k_\theta = 10$ rad^{-2} here. The angle θ between the two molecules adopts the preferred value $\theta_0 = 0$ if the two molecules are facing each other. The binding potential attains its minimum value of $-\frac{1}{2}F_m\, r_0 = -8\, k_B T$ at $r = r_0$ and $\theta = \theta_0$. For this intermediate binding energy of the receptors and ligands, both stable bonds and a large number of binding and unbinding events can be observed in our simulations.

DPD Simulations. In each simulation, the number density of DPD beads in the rectangular simulation box of size $V = L_x \times L_y \times L_z$ is set to $\rho = 3\, r_0^{-3}$. The total number of beads in each simulation system thus is ρV. The Newton's equations of motion are numerically integrated with a time step $t_0 = 0.03\sqrt{m_0 r_0^2/k_B T}$ using the velocity-Verlet algorithm as in ref. 3. For this time step, the average temperature of the beads deviates from the expected value by at most 2%. Our optimized DPD code is parallelized to achieve a speedup of about a factor 6 by using eight central processing unit (CPU) cores, which enables us to simulate up to tens of thousands of binding and unbinding events to determine the binding constants with high accuracy. A relaxation run of $2 - 5 \cdot 10^6\, t_0$ is performed for thermal equilibrium in each system before statistical sampling.

Physical length and time scales for the bead diameter r_0 and for the step width t_0 of our simulations can be obtained from a comparison with experimental data for dimyristoyl-phosphatidylcholine (DMPC) bilayers (6, 7). Our model lipids correspond to the phospholipid DMPC as each C bead of the lipid tails can be seen to represent 3.5 CH$_2$ groups (4, 6), which leads to a total tail length of 14 CH$_2$ groups as for DMPC. To obtain a physical length scale for the bead diameter r_0, we compare experimental data for the thickness of fluid DMPC bilayers or, more precisely, for the vertical distance d_{HH} between the head groups of the two monolayers. From the experimental value $d_{HH} \simeq 3.53$ nm (8) and our simulation result $d_{HH} \simeq 3.64\, r_0$, we obtain the physical length scale $r_0 \simeq 1.0$ nm. From a comparison of the experimentally measured lateral diffusion coefficient $D \simeq 5\, \mu\text{m}^2/\text{s}$ of DMPC (9) to our simulation result $D \simeq 5.7 \cdot 10^{-4} r_0^2/t_0$, we obtain the physical time scale $t_0 \simeq 0.114$ ns.

Simulations with Confining Potentials. In our simulations with confining membrane potentials, we impose additional harmonic potentials

$$V_{conf}(z) = \frac{1}{2}k_{conf}(z - z_0)^2 \qquad \textbf{[S10]}$$

on one of the three head beads of each lipid in the two distal monolayers of the apposing membranes—that is, in the two monolayers that do not face the other membrane. The potential is imposed on the head bead that is connected to the left side chain of the lipid molecule shown in Fig. 1A. The z-direction of our simulation box is on average perpendicular to the membranes. The three red data points in Fig. 4 are from simulations with the rather weak confining strengths $k_{conf} = 1, 2$ and $4\, k_B T/\text{nm}^2$ (from

right to left). The membrane tensions in these simulations are 0.13 ± 0.02, -0.15 ± 0.03, and $-0.49 \pm 0.01\, k_B T/\text{nm}^2$ for the confining strengths 1, 2, and $4\, k_B T/\text{nm}^2$, respectively.

Analysis of Binding Kinetics

Maximum-Likelihood Estimation of Rate Constants. We complement here the analysis of the binding kinetics described in the main text by (i) a derivation of the time-dependent probability $P_n(t)$ of a state with n receptor–ligand bonds and (ii) an estimation of the errors for the rate constants obtained by this analysis.

In Fig. S2A, the number of bonds n is displayed as a function of time for a short segment of a simulation trajectory of our largest membrane system with 15 receptors and 15 ligands. A central quantity for extracting the binding kinetics from our simulation trajectories is the probability $P_n(t)$ of staying for a dwell time t in state n. For a Markov process, we have

$$P_n(t + \Delta t) = P_n(t)P_n(t + \Delta t | t), \qquad \textbf{[S11]}$$

where $P_n(t + \Delta t | t)$ is the conditional probability of remaining in state n from time t to $t + \Delta t$. For small time windows Δt, this probability is

$$P_n(t + \Delta t | t) = 1 - \left[k_+^{(n)} + k_-^{(n)} \right] \Delta t, \qquad \textbf{[S12]}$$

where $k_+^{(n)}$ is the transition rate from state n to state $n + 1$, and $k_-^{(n)}$ is the transition rate from state n to state $n - 1$. The probabilities of transitions from state n to states $n \pm 2, n \pm 3, \dots$ are negligible for small Δt. From Eqs. S11 and S12, we obtain

$$\frac{P_n(t + \Delta t) - P_n(t)}{\Delta t} = -P_n(t)\left[k_+^{(n)} + k_-^{(n)} \right], \qquad \textbf{[S13]}$$

which leads to

$$\frac{dP_n(t)}{dt} = -P_n(t)\left[k_+^{(n)} + k_-^{(n)} \right] \qquad \textbf{[S14]}$$

for $\Delta t \to 0$. The solution of Eq. S14 is the exponential dwell-time distribution

$$P_n(t) = e^{-\left[k_+^{(n)} + k_-^{(n)} \right]t}. \qquad \textbf{[S15]}$$

Fig. S2B illustrates that the histogram of dwell times in state $n = 5$ obtained from our DPD simulations with 15 anchored receptors and ligands fits well to an exponential distribution.

The variances $\delta^2 k$ of the maximum likelihood estimators can be estimated by the Cramer–Rao lower bound $\delta^2 k = (-d^2 \ln L/dk^2)^{-1}$ (10). For the likelihood function L given in Eq. 17 and $k = k_{on}^{(n)}$ or $k_{off}^{(n)}$ given in Eq. 18, we obtain as errors of our rate constant estimates

$$\delta k_{on}^{(n)} \simeq \frac{k_{on}^{(n)}}{\sqrt{N_n^+}} \qquad \textbf{[S16]}$$

and

$$\delta k_{off}^{(n)} \simeq \frac{k_{off}^{(n)}}{\sqrt{N_n^-}}. \qquad \textbf{[S17]}$$

Binding of Soluble Receptors and Ligands. In addition to the membrane systems described in the main text, we have determined the binding kinetics of soluble receptor and ligand molecules that lack the transmembrane anchor. We have considered a single soluble receptor and a single soluble ligand randomly placed in water contained in simulation boxes with the four different sizes $L_x = L_y = L_z = 20$ nm, 24 nm, 28 nm, and 32 nm. Within the statistical errors, the 3D on- and off-rate constants

k_{on} and k_{off} and the binding equilibrium constant K_{3D} are independent of the box size (Fig. S3). We obtain the estimates $k_{on} = (6.2 \pm 0.2) \cdot 10^7 \text{nm}^3/\text{s}$, $k_{off} = (4.0 \pm 0.1) \cdot 10^5/\text{s}$, and $K_{3D} = (157 \pm 6) \text{nm}^3$.

Receptors and Ligands with Increased Binding Energy. To illustrate that our general results for the ratio of K_{2D} and K_{3D} do not depend on the values of the on- and off-rate constants or binding constants, we have performed additional simulations in which the binding strength F_m of the receptors and ligands is increased from our standard value $16 k_B T/r_0$ (Eq. S8) to the value $20 k_B T/r_0$. For the larger binding strength $20 k_B T/r_0$, we obtain the binding constant $K_{3D} = (537 \pm 23) \text{nm}^3$ and the rate constants $k_{on} = (6.6 \pm 0.2) \cdot 10^7 \text{nm}^3/\text{s}$ and $k_{off} = (1.23 \pm 0.04) \cdot 10^5/\text{s}$ of our soluble receptors and ligands. The increase in the binding strength and binding energy by 25% thus increases the binding constant K_{3D} by a factor 3.4 ± 0.2, mainly due to a decrease in the off-rate k_{off}. From simulations with tensionless membranes of area $14 \times 14 \text{ nm}^2$ at the optimal membrane separation, we obtain the value $K_{2D} = (2820 \pm 60) \text{nm}^2$ for the binding strength $20 k_B T/r_0$, which is a factor 3.4 ± 0.1 larger than the value $K_{2D} = (829 \pm 12) \text{nm}^2$ for this membrane system from simulations with our standard binding strength $16 k_B T/r_0$ (see dark blue data point indicated by the left arrow in Fig. 4). The relative membrane roughness $\xi_\perp$ is determined by the membrane area in this system and, thus, independent of the binding strength within numerical accuracy. Because the increase in the binding strength increases both K_{2D} and K_{3D} by the same factor, the ratio K_{2D}/K_{3D} of the binding constants does not change. For the increased binding strength $20 k_B T/r_0$, the rate constants of the membrane-anchored receptors and ligands are $k_{on} = (7.6 \pm 0.1) \cdot 10^7 \text{nm}^2/\text{s}$ and $k_{off} = (2.69 \pm 0.04) \cdot 10^4/\text{s}$ in this membrane system. For our standard binding strength $16 k_B T/r_0$, these rate constants are $k_{on} = (7.3 \pm 0.1) \cdot 10^7 \text{nm}^2/\text{s}$ and $k_{off} = (8.8 \pm 0.1) \cdot 10^4/\text{s}$.

Calculation of Binding Free Energies

Binding Free Energy of Soluble Receptors and Ligands. The binding equilibrium constant K_{3D} of a single soluble receptor and a single soluble ligand molecule in a volume V is related to the binding free energy ΔG_{3D} of the molecules via Eq. 2. The binding free energy can be written as

$$\Delta G_{3D} = -k_B T(\ln Z_b - \ln Z_u), \qquad \textbf{[S18]}$$

where Z_b and Z_u are the configurational integrals in the bound and unbound state of the molecules. For rod-like receptors and ligands, the configurational integral in the unbound state is

$$Z_u \simeq 2\pi V \int_0^\pi \sin\theta d\theta = 4\pi V \qquad \textbf{[S19]}$$

in the dilute limit $V \to \infty$, where θ is the angle between the two molecules. The configurational integral in the unbound state is the product of the translational phase space volume V and the rotational phase space volume 4π of the unbound receptor relative to the ligand.

To calculate the configurational integral Z_b in the bound state of the molecules, we follow a standard approach that is based on a harmonic expansion of the potential of mean force $U(r_x, r_y, r_z, \theta)$ between the interaction beads of the two bound molecules around its minimum U_0 (11, 12):

$$U(r_x, r_y, r_z, \theta) \simeq U_0 + \sum_{q=x,y,z} \frac{k_q}{2}(r_q - r_{q,0})^2 + \frac{k'_\theta}{2}\theta^2. \qquad \textbf{[S20]}$$

Here, (r_x, r_y, r_z) is the distance vector between the beads. For definiteness, we assume that the z-direction is parallel to the

ligand, and thus, on average parallel to the receptor–ligand complex, which attains its potential minimum for $\theta = 0$—that is, for a collinear orientation of the receptor and ligand. With Eq. S20, the configurational integral in the bound state can be approximated as

$$Z_b \simeq e^{-U_0/k_B T} Z_{trans} Z_{rot}, \qquad \textbf{[S21]}$$

with the translational integral

$$Z_{trans} \simeq \prod_{q=x,y,z} \int_{-\infty}^\infty e^{-\frac{1}{2}k_q(r_q - r_{q,0})^2/k_B T} dr_q = (2\pi)^{3/2} \xi_x \xi_y \xi_z \qquad \textbf{[S22]}$$

and the rotational integral

$$Z_{rot} \simeq 2\pi \int_0^\pi e^{-\frac{1}{2}k'_\theta\theta^2/k_B T} \sin\theta d\theta \simeq 2\pi\sigma_b^2 \quad \text{for} \quad k'_\theta \gg k_B T. \qquad \textbf{[S23]}$$

Here, $\xi_q = (k_B T/k_q)^{1/2}$ and $\sigma_b = (k_B T/k'_\theta)^{1/2}$ are the SDs of the Gaussian distributions for the coordinates $q = x, y, z$ of the binding vector and the binding angle θ, which result from the harmonic approximation of the potential of mean force in Eq. S20. The integrals Z_{trans} and Z_{rot} involve three translational and two rotational degrees of freedom. Based on these integrals, the binding free energy ΔG_{3D} defined in Eq. S18 can be written as

$$\Delta G_{3D} \simeq U_0 + \Delta G_{trans} + \Delta G_{rot}, \qquad \textbf{[S24]}$$

with the change $\Delta G_{trans} = -k_B T \ln(Z_{trans}/V)$ in translational free energy and the change $\Delta G_{rot} = -k_B T \ln(Z_{rot}/4\pi)$ in rotational free energy during binding.

We now decompose the translational free-energy change ΔG_{trans} into (*i*) an entropic contribution

$$-T\Delta S_{trans} = T \frac{\partial \Delta G_{trans}}{\partial T} = -k_B T \ln\left[\frac{V_b}{V}\right] \qquad \textbf{[S25]}$$

with the bound-state translational phase space volume

$$V_b = e^{3/2} Z_{trans} = (2\pi e)^{3/2} \xi_x \xi_y \xi_z \qquad \textbf{[S26]}$$

and (*ii*) an enthalpic contribution $\Delta U_{trans} = \Delta G_{trans} + T\Delta S_{trans} = \frac{3}{2}k_B T$. The factor $e^{3/2}$ in Eq. S26 results from the temperature dependence of the SDs ξ_x, ξ_y, and ξ_z. Similarly, we decompose the rotational free-energy change ΔG_{rot} into (*i*) an entropic contribution

$$-T\Delta S_{rot} = T\partial\Delta G_{rot}/\partial T = -k_B T \ln[\omega_b/4\pi] \qquad \textbf{[S27]}$$

with the bound-state rotational phase space volume

$$\omega_b = eZ_{rot} = 2\pi e\sigma_b^2 \qquad \textbf{[S28]}$$

and (*ii*) an enthalpic contribution $\Delta U_{rot} = \Delta G_{rot} + T\Delta S_{rot} = k_B T$. The binding free energy ΔG_{3D} then can be written as the sum of enthalpic and entropic contributions as in Eq. 3 with the binding enthalpy

$$\Delta U = U_0 + \Delta U_{trans} + \Delta U_{rot} = U_0 + \frac{5}{2}k_B T. \qquad \textbf{[S29]}$$

Binding Free Energy of Membrane-Anchored Receptors and Ligands. Analogous to the case of soluble molecules, we now consider a single receptor and a single ligand that are anchored in two apposing membranes of area A. Our aim is to decompose the binding free energy ΔG_{2D}, which is related to the apparent

binding constant K_{2D} of the molecules via Eq. **5**, into the sum of an enthalpic contribution ΔU and entropic contributions. We assume that the binding interface of the membrane-anchored molecules is identical with the binding interface of the soluble counterparts of the molecules, which lack the membrane anchors (13). This assumption is supported by the distributions of binding distances and angles for our soluble and membrane-anchored receptor–ligand complexes (Fig. S4). The binding enthalpy ΔU of the membrane-anchored receptor and ligand molecules is then identical to the binding enthalpy of the soluble molecules.

Because the anchored molecules diffuse along the membranes, the free-energy contribution from the translational entropy change during binding is

$$-T\Delta S_{\text{trans}} \simeq -k_B T \, \ln\left[\frac{A_b}{A}\right], \qquad \textbf{[S30]}$$

where A_b is the translational area of the bound receptor–ligand complex in analogy to Eq. **S25**. The two membranes are on average perpendicular to the receptor–ligand complex. In analogy to Eq. **S26**, the bound-state translational area of the complex is then:

$$A_b = 2\pi e \xi_x \xi_y, \qquad \textbf{[S31]}$$

where ξ_x and ξ_y are the SDs of the binding vector coordinates in the two directions perpendicular to the complex and parallel to the membranes. In our simulations, the distributions of the binding vector coordinates x and y perpendicular to the complex are identical for the soluble and anchored molecules (Fig. S4A).

In analogy to Eqs. **S27** and **S28**, the free-energy contribution from rotational entropy changes of the anchored molecules can be calculated as

$$-T\Delta S_{\text{rot}} = -k_B T \, \ln\left[\frac{\omega_b \omega_{\text{RL}}}{\omega_R \omega_L}\right], \qquad \textbf{[S32]}$$

where $\omega_R = 2\pi e \sigma_R^2$ and $\omega_L = 2\pi e \sigma_L^2$ are the rotational phase space volumes of the unbound receptor and unbound ligand relative to the membrane, and $\omega_{\text{RL}} = 2\pi e \sigma_{\text{RL}}^2$ is the rotational phase space volume for the bound receptor or bound ligand relative to the membrane. Here, σ_R, σ_L, and σ_{RL} are the SDs of the anchoring angle distributions for the unbound and bound receptor and ligand molecules shown in Fig. S5. Eq. **S32** implies that the binding angle distribution is significantly narrower than the anchoring angle distribution of the bound receptors and ligands. The binding angle distribution then is not affected by the anchoring and is practically identical for the soluble and anchored molecules (Fig. S4). Because the rotational degrees of freedom for the binding angle thus are independent from the anchor rotations, the overall rotational phase space volume for the receptor–ligand complex is the product of the volume ω_{RL} for the rotation of the receptor (or ligand) relative to the membrane and the volume ω_b of the ligand (or receptor) relative to its binding partner. Because our receptor

and ligand molecules have identical anchors, the rotational phase space volume ω_{RL} is identical for the ligand or receptor. However, Eq. **S32** should also hold for different anchoring of receptors and ligands if the binding angle distribution is sufficiently narrow. The receptor–ligand complex is then rather stiff, and the anchoring angles for the receptor and ligand are rather similar because the membranes are on average parallel.

In addition to the translational and rotational entropy loss ΔS_{trans} and ΔS_{rot} of the molecules, the binding of anchored receptor and anchored ligand molecules also leads to an entropy loss ΔS_{mem} of the membranes, as the bound receptor–ligand complex constrains the membrane shape fluctuations. Here, we approximate the receptor–ligand complex as a harmonic constraint $(b/2)l_i^2$ of the local membrane separation l_i with strength b. For such a harmonic constraint, the purely entropic free-energy change of the membrane has been calculated exactly as (14)

$$-T\Delta S_{\text{mem}} = \frac{k_B T}{2} \ln\left[1 + \frac{b\xi_\perp^2}{kT}\right] = \frac{k_B T}{2} \ln\left[1 + \frac{\xi_\perp^2}{\xi_{\text{RL}}^2}\right], \qquad \textbf{[S33]}$$

where $\xi_{\text{RL}} = \sqrt{kT/b}$ is the SD for fluctuations of the local separation l_i within the harmonic constraint. With Eqs. **S30**, **S32**, and **S33**, we obtain the decomposition of the binding free energy ΔG_{2D} of the anchored receptors and ligands given in Eq. **6**.

Results for Our Model. In our harmonic approximation, the changes in rotational and translational entropy during binding of receptors and ligands depend on the SDs of the binding vector coordinates, binding angles, and anchoring angles. For our receptors and ligands, these SDs can be calculated from the distributions shown in Figs. S4 and S5. For the soluble receptors and ligands, we obtain the SDs $\xi_x = \xi_y \simeq 0.52$ nm for the binding vector coordinates r_x and r_y in the two directions perpendicular to the receptor–ligand complex from Fig. S4A and the SD $\xi_z \simeq 0.19$ nm for the coordinate r_z parallel to the complex from Fig. S4B. These SDs lead to the estimate $V_b \simeq 3.6$ nm^3 for the translational phase space volume of the bound receptor relative to the ligand (Eq. **S26**). From the binding angle distribution shown in Fig. S4C, we obtain the SD $\sigma_b \simeq 0.084$, which leads to the estimate $\omega_b \simeq 0.12$ for the rotational phase space volume of the bound receptor relative to the ligand.

The distributions of the binding vector coordinates r_x and r_y and the binding angle θ are practically identical for the soluble and anchored receptors and ligands. From the values $\xi_x = \xi_y \simeq 0.52$ nm for the SDs of r_x and r_y, we obtain the estimate $A_b \simeq 4.6$ nm^2 for the translational phase space area of the anchored receptor–ligand complex (Eq. **S31**) and the estimate $\xi_b = V_b/A_b \simeq 0.78$ nm. From the SDs $\sigma_R = \sigma_L \simeq 0.21$ and $\sigma_{\text{RL}} \simeq 0.14$ of the anchoring angle distributions for the unbound and bound receptor and ligand molecules shown in Fig. S5, we obtain the estimates $\omega_R = \omega_L \simeq 0.75$ and $\omega_{\text{RL}} \simeq 0.33$ for the rotational phase space volumes of the molecules.

1. Hoogerbrugge PJ, Koelman JMVA (1992) Simulating microscopic hydrodynamic phenomena with dissipative particle dynamics. *Europhys Lett* 19(3):155–160.
2. Espanol P, Warren P (1995) Statistical mechanics of dissipative particle dynamics. *Europhys Lett* 30(4):191–196.
3. Groot RD, Warren PB (1997) Dissipative particle dynamics: Bridging the gap between atomistic and mesoscopic simulation. *J Chem Phys* 107(11):4423–4435.
4. Goetz R, Lipowsky R (1998) Computer simulations of bilayer membranes: Self-assembly and interfacial tension. *J Chem Phys* 108(17):7397–7409.
5. Shillcock JC, Lipowsky R (2002) Equilibrium structure and lateral stress distribution of amphiphilic bilayers from dissipative particle dynamics simulations. *J Chem Phys* 117(11):5048–5061.
6. Grafmüller A, Shillcock J, Lipowsky R (2007) Pathway of membrane fusion with two tension-dependent energy barriers. *Phys Rev Lett* 98(21):218101.
7. Grafmüller A, Shillcock J, Lipowsky R (2009) The fusion of membranes and vesicles: Pathway and energy barriers from dissipative particle dynamics. *Biophys J* 96(7):2658–2675.
8. Kucerka N, et al. (2005) Structure of fully hydrated fluid phase DMPC and DLPC lipid bilayers using X-ray scattering from oriented multilamellar arrays and from unilamellar vesicles. *Biophys J* 88(4):2626–2637.
9. Orädd G, Lindblom G, Westerman PW (2002) Lateral diffusion of cholesterol and dimyristoylphosphatidylcholine in a lipid bilayer measured by pulsed field gradient NMR spectroscopy. *Biophys J* 83(5):2702–2704.
10. Kay SM (1993) *Fundamentals of Statistical Signal Processing, Volume I: Estimation Theory* (Prentice Hall, Englewood Cliffs, NJ).
11. Luo H, Sharp K (2002) On the calculation of absolute macromolecular binding free energies. *Proc Natl Acad Sci USA* 99(16):10399–10404.
12. Woo H-J, Roux B (2005) Calculation of absolute protein-ligand binding free energy from computer simulations. *Proc Natl Acad Sci USA* 102(19):6825–6830.
13. Wu Y, Vendome J, Shapiro L, Ben-Shaul A, Honig B (2011) Transforming binding affinities from three dimensions to two with application to cadherin clustering. *Nature* 475(7357):510–513.
14. Netz RR (1997) Inclusions in fluctuating membranes: Exact results. *J Phys I* 7(7):833–852.
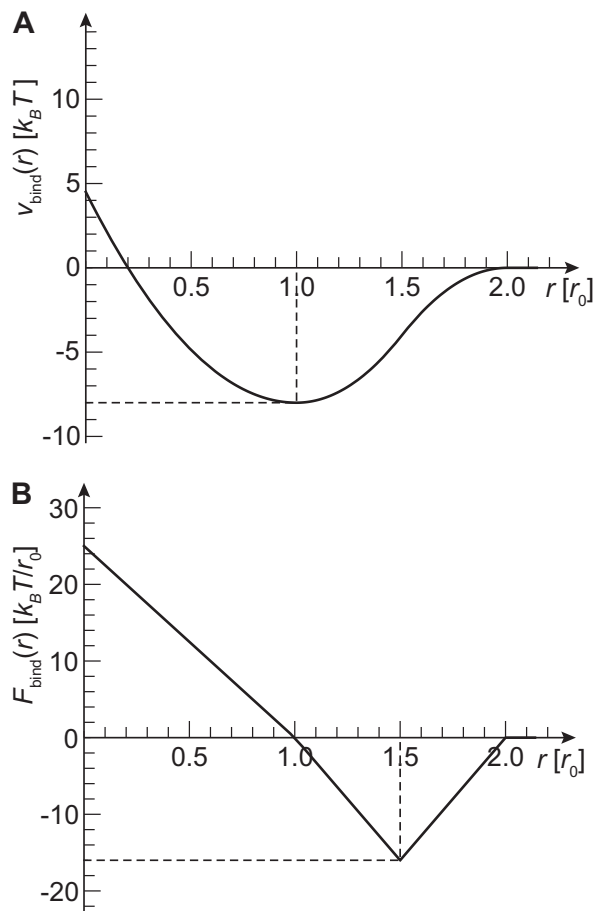
Fig. S1. (A) The distance-dependent term $v_{bind}(r)$ of the binding potential between the interaction beads of receptor and ligand molecules (Eq. **S8**). The minimum of the binding potential is −8 $k_B T$. (B) The radial force component corresponding to $v_{bind}(r)$ (Eq. **S9**).
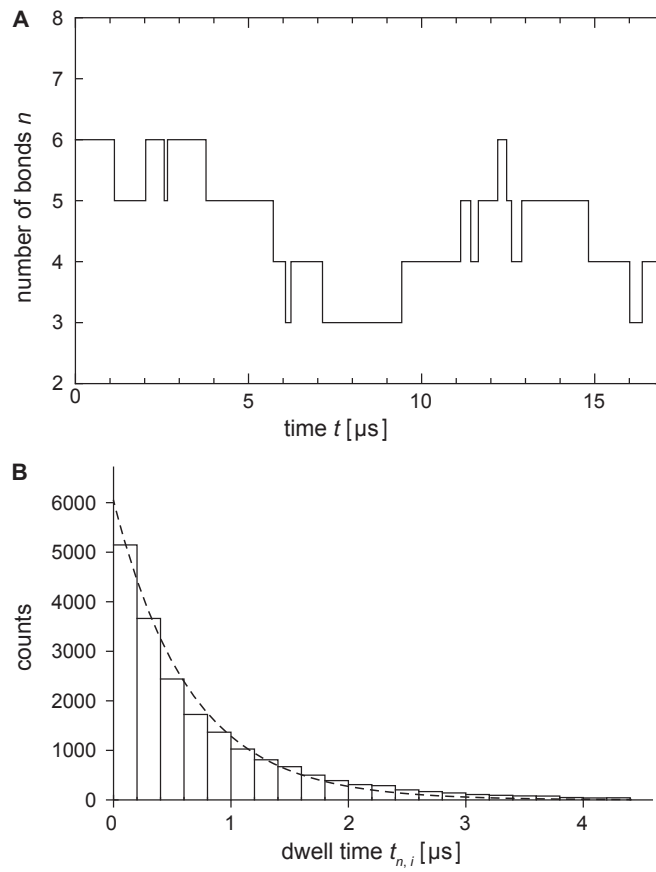
Fig. S2. (*A*) Number of receptor–ligand bonds n as a function of time t for a short time interval of a simulation with 15 anchored receptors and 15 ligands. (*B*) Dwell-time probabilities in state $n = 5$ obtained from our simulations with 15 anchored receptors and ligands. The dashed line results from an exponential fit.
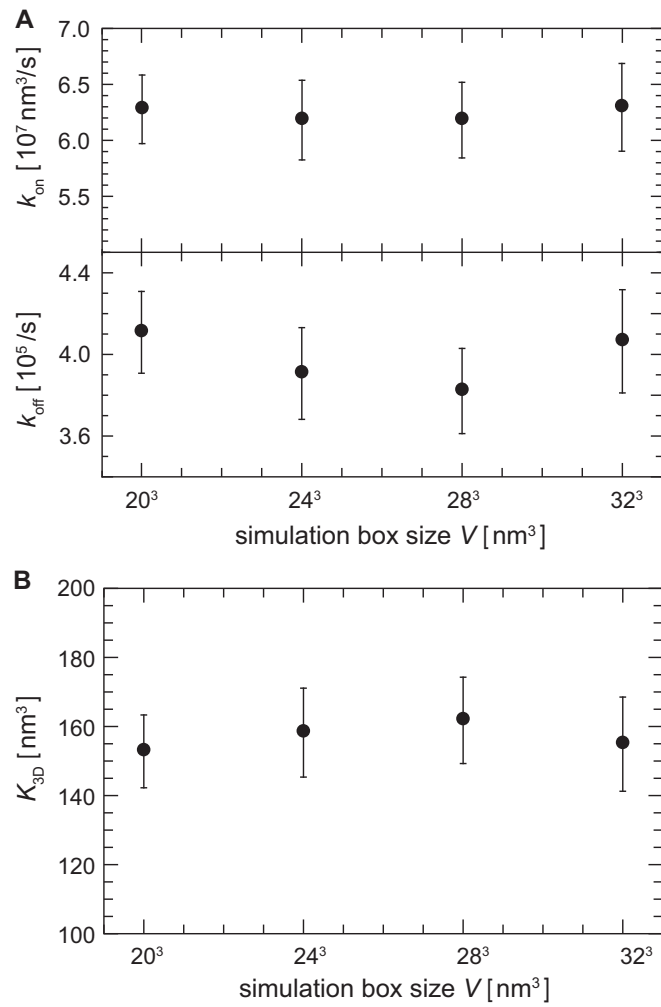
Fig. S3. (A) 3D on- and off-rate constants k_{on} and k_{off} and (B) binding equilibrium constant $K_{3D} = k_{on}/k_{off}$ obtained from DPD simulations with a single soluble receptor and a single soluble ligand in cubic simulation boxes of different volume V.
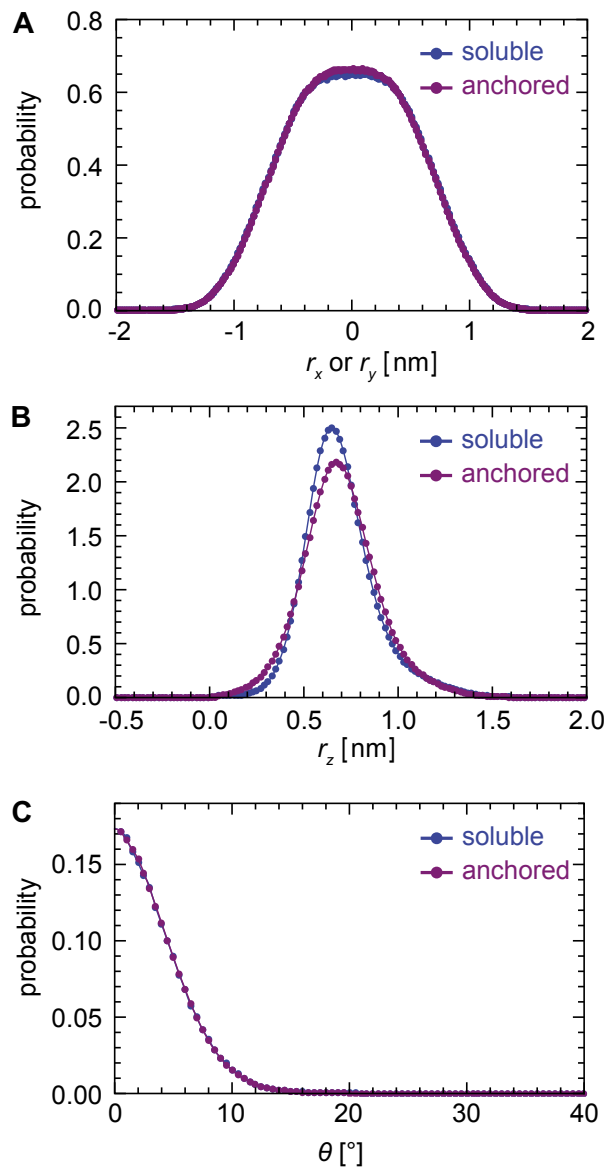
Fig. S4. (A) Probability distributions of the binding vector coordinates r_x and r_y in the two directions perpendicular to the receptor–ligand complex of our soluble and anchored molecules. (B) Distributions of the binding vector coordinate r_z in the direction parallel to the complex. (C) Distributions of the binding angle θ of our soluble and anchored receptor–ligand complexes.
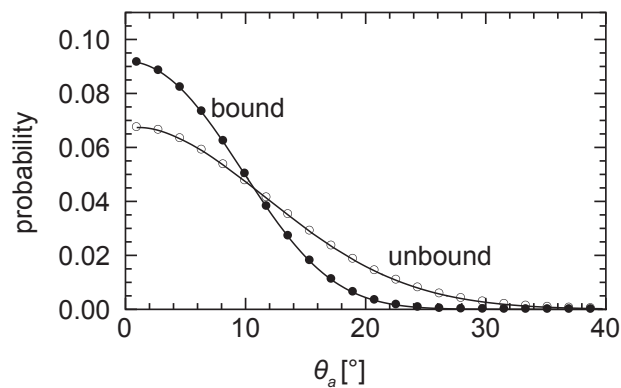
Fig. S5. Probability distributions of the anchoring angle θ_a between the unbound and bound receptors and ligands and the membrane normal.

Table S1. DPD repulsion strength a_{ij} in units of $k_B T/r_0$

Bead type	W	H	C	T_H	T_C	I
W	25	30	75	30	75	25
H	30	30	35	30	35	30
C	75	35	10	35	10	35
T_H	30	30	35	25(75)	25(75)	25(75)
T_C	75	35	10	25(75)	25(75)	25(75)
I	25	30	35	25(75)	25(75)	25(75)

Numbers in parentheses indicate the repulsion strength between the beads of two different receptors or two different ligands.